

The Reliability of Single-Step and Double-Step Quench and Partitioning Heat Treatments on an AISI 420A Low Carbon Martensitic Stainless Steel



S. BARELLA, A. GRUTTADAURIA, J.T.O. MENEZES, E.M. CASTRODEZA, S.E. QUAINI, C. PELLIGRA, and E.A. MCNALLY

The microstructural and mechanical effects of various single-step (SS) and double-step (DS) quench and partition (Q&P) heat treatments applied to an AISI 420A low carbon martensitic stainless steel (MSS) has been studied. The goal with this work is to reach a total elongation (E pct) of 12 pct and an ultimate tensile strength (UTS) above 1200/1300 MPa, but ultimately to achieve a superior strength-ductility balance in comparison to its traditional Quench and Temper (Q&T) counterpart. This is being done by retaining austenite within the steel's martensitic matrix at room temperature (RT) using novel SS and conventional DS Q&P heat treatments. Considerable work has been done to optimize DS Q&P heat treatments, but little has been done to understand the effects of removing a subsequent heating cycle through SS Q&P heat treatments has on MSSs. With that being said, partitioning is performed at the same quench interruption temperature for the SS Q&P heat treatments, and reheated to a higher temperature for the DS Q&P heat treatments. Experimental investigations were carried out on 1 mm thick, sheet samples to increase the number of potential applications for this steel and heat treatment. The microstructure of different SS and DS Q&P heat treatments was investigated through X-ray diffraction (XRD) and transmission electron microscopy (TEM) while mechanical property investigations were carried out using tensile and fracture toughness testing. DS Q&P heat treated samples quenched to 130 °C and partitioned for industrially relevant times of 10 and 30 minutes featured the highest values in terms of total elongation, tensile strength and fracture toughness. The SS Q&P heat treatments, on the other hand, were able to achieve improved mechanical properties to its Q&T counterpart. Overall, this work opens up the possibility of increased MSS usage for reliable, thin-walled component production with improved properties through Q&P heat treatment methods. The best results achieved in this study are a UTS of 1585 MPa, E pct of 22 pct, and a fracture toughness of 77 kJ/m². Their lower total elongation of 9.6 pct is balanced by high tensile strength of 1812 MPa, ensuring higher toughness compared to traditional Q&T samples.

<https://doi.org/10.1007/s11661-023-07145-2>

© The Author(s) 2023

I. INTRODUCTION

QUENCH and partitioning of steels is a possible method to create high-strength products with high formability without significantly increasing steel weight,

production costs, and alloying elements. Quench and partition (Q&P) steels can be obtained by single-step (SS) and double-step (DS) heat treatments. The former process removes a second heating cycle, resulting in lower overall energy consumption, which is desirable from an industrial perspective as financial and environmental costs can be reduced. In comparison to traditional processes, a Q&P heat treatment allows thin-walled components and structures to be produced without affecting its structural integrity. It is important, for example, for the automotive industry in which lighter components improves fuel efficiency and reduces greenhouse gas emissions.^[1-5]

Q&P steels result in outstanding, tailorable properties as a result of its composite-like microstructures containing submicron, decarburized martensite (M) laths,

S. BARELLA, A. GRUTTADAURIA, J.T.O. MENEZES, E.M. CASTRODEZA, and S.E. QUAINI are with the Department of Mechanical Engineering, Politecnico di Milano, Via G. La Masa 34, 20156 Milan, MI, Italy. Contact e-mail: silvia.barella@polimi.it C. PELLIGRA and E.A. MCNALLY are with the Department of Materials Science and Engineering, McMaster University, 1280 Main Street West, JHE 357, Hamilton ON, Canada.

Manuscript submitted February 17, 2023; accepted July 14, 2023.

Article published online July 30, 2023

Table I. AISI 420A Low Carbon MSS Chemical Composition (Wt Pct).

C	Cr	Si	Mn	Ni	Mo	Cu	Ti	S	P	Al	V	Co	Nb	Fe
0.21	13.23	0.54	0.32	0.2	0.02	0.18	0.006	0.001	0.031	0.001	0.087	0.01	0.01	bal.

carbon-enriched M plates, nanoscale retained austenite (RA) thin-films and nanoscale transitional carbides. Unfortunately, the successful development of Q&P heat treated steels is not trivial because of the RA fraction and its stability are controlled by the steel's carbon (C) content.^[6-9] As proposed by Speer *et al.* in 2005,^[10-13] during a Q&P heat treatment, RA is deliberately introduced within M laths or packets and then stabilized thanks to the C migration from the supersaturated M to RA.

To obtain higher fractions of RA in Q&P heat treatments, alloying elements, such as; Mn and Si, are required. The former is used to stabilize the RA and the latter to retard carbide formation. C is also fundamental for the martensite formation and the stabilization of the RA in the partitioning step. Yet, a Q&P heat treatment is a simple multi-step processing route suitable for any quenchable metal. The first step in a Q&P heat treatment is austenitization or intercritical annealing, followed by quenching to an interruption temperature between the start and finish temperatures of the martensitic transformation (M_s and M_f , respectively). Interrupting a quench at a temperature between the M_s and M_f allows the fraction of M and RA within the structure to be somewhat controlled. The M_f must be above room temperature (RT) when performing a Q&P heat treatment. In the case of SS Q&P heat treatments, the steel is held at the quench interruption temperature for an ideal partitioning time whereas, in DS Q&P heat treatments, the steel is reheated to a temperature above the M_s for an ideal partitioning time. With that being said, partitioning time is also an important parameter in both SS and DS Q&P heat treatments in order to enable sufficient RA carbon enrichment and stabilization at RT.^[14] During deformation, the RA is expected to transform into M, which ultimately can delay the onset of necking and improve steel elongation through the transformation induced plasticity effect (TRIP).^[13,15-18] The overall goal with Q&P heat treatments on martensitic stainless steels (MSSs) is to reach a total elongation (E pct) of 12 pct and an ultimate tensile strength (UTS) above 1200/1300 MPa.^[8,19-22]

Despite a lot research done on applying DS Q&P heat treatments on carbon steels, only a few investigations have been focused on applying a Q&P heat treatment to MSSs.^[23] For example, Tobata *et al.*^[12] show the increase in ductility of the Q&P AISI 410 grades of about 5 pct in relation to its Quench and Temper (Q&T) condition. Other works explain some mechanisms correlated to the microstructure evolution in Q&P MSSs. In Reference [10] the authors have demonstrated the presence of M_3C in Q&P AISI 410 that can form after a partitioning time of 10 minutes at 450 °C, but the presence of Cr is also able to reduce the thermodynamic

activity of carbon. Other studies have demonstrated that the effect of Cr is similar to that of Si and is able to increase the amount of the RA.^[24,25]

Potential applications for lightweight MSSs are in the automotive sector, including parts requiring high energy absorption in the elastic and low-plastic range, such as automotive sub-frames and B-pillar reinforcements.^[26] In addition, automotive MSS components may be suitable as deep-drawn parts. Applying a Q&P heat treatment to MSSs can be advantageous, for example, in battery-powered electric vehicles (BEV) in which a battery holder can be designed as a deep-drawn shell solution.^[27] Moreover, a significant amount of space can be occupied by a vehicle's battery and complex design procedures of the battery is required. MSSs offers the ability for these batteries to be protected from environmental corrosion, high temperatures, stone chips as well as deformation, to prevent thermal collapse. Furthermore, sustaining crushes, especially for side and under-floor intrusion, is a big challenge.^[4] Other than the automotive applications, Q&P heat treatments have been applied to martensitic steels serving the aerospace and defense industries.^[28]

This work investigates the reliability of performing SS and DS Q&P heat treatments on an AISI 420A low carbon MSS with limited elongation properties. This study was conducted using flat and thin samples which can influence the measurement of bulk mechanical properties but are fundamental in light weighting of final components. An understanding of the structural integrity of these steels requires an evaluation of both their tensile mechanical properties and fracture toughness, which were determined using testing standards. In addition, microstructural characterization of the steel was performed with X-ray diffraction (XRD) and transmission electron microscopy (TEM).

II. EXPERIMENTAL PROCEDURE

A. As-Received Steel and Dilatometry

The chemical composition of the commercialized AISI 420A low carbon MSS studied in this investigation was determined using an Optical Emission Spectrometer (OES) Sirio Analytix/Bruker Q4 Tasman 170, as shown in Table I. The majority of experiments carried out in this paper were performed using 1.0 mm thick, sheet samples with the exception of dilatometry. After grinding and polishing through standardized metallographic procedures and chemical etching with Aqua Regia (1:1:1 H₂O, HCl, HNO₃), the as-received microstructure revealed annealed equiaxed ferrite with a dispersion of $M_{23}C_6$ spheroidized carbides.

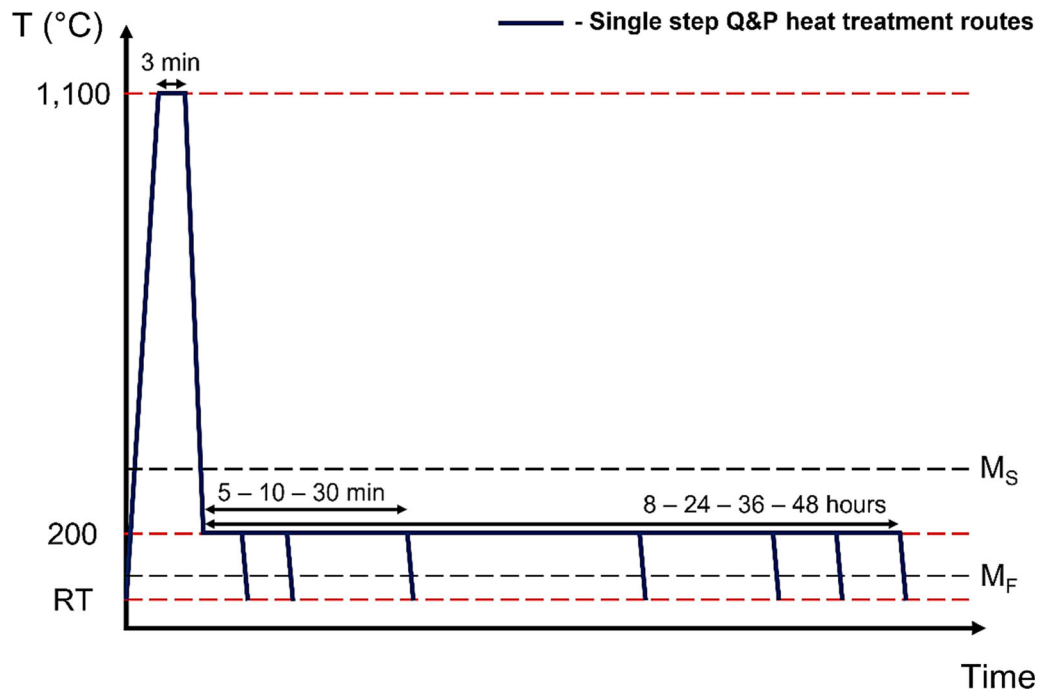


Fig. 1—Schematic representation of the experimental single-step (SS) Q&P heat treatments.

Before performing any SS and DS Q&P heat treatments, dilatometry was performed to validate the selected quench and partitioning temperatures. Cylindrical samples, 9.20 ± 0.05 mm in length and 4.0 mm in diameter, were machined from 10.0 mm thick bars. The samples were heated up at a rate of 20 °C/s to 900 °C or 1050 °C, held for 3 or 5 minutes, and then quenched with helium at a rate of 80 °C/s to RT to obtain a homogenized austenitic microstructure and to measure Ac_1 and Ac_3 . After that, the samples were heated to 1050 °C, quenched to either 130 °C or 200 °C, held at that temperature for 1 minutes and then, depending on the Q&P heat treatment, reheated to 450 °C or maintained at 200 °C to perform partitioning. According to Wendler *et al.*,^[17] the temperature to enable partitioning of interstitial elements is at 450 °C, hence it's use in this study for DS Q&P heat treatments.

B. Q&P Heat Treatments

Q&P heat treatment temperatures were chosen based off of ThermoCalc simulations and the dilatometric analysis. The challenging SS Q&P heat treatment, desired for potential energy savings, was investigated with a focused goal of optimizing partitioning time rather than temperature. Using ThermoCalc software, quench and partitioning temperatures were found to coincide at 200 °C, making it also the partitioning temperature used for SS Q&P experiments. Samples were first austenitized at 1100 °C for 3 minutes to obtain a homogenized microstructure and to dissolve Cr-rich carbides,^[29-31] then quenched to 200 °C in an oil bath. These samples were held in the oil bath at 200 °C for partitioning times varying from 1 minutes to 48 hours followed by a water quench to RT, as illustrated in Figure 1.

Samples subjected to DS Q&P heat treatments were also initially austenitized at 1100 °C for 3 minutes then quenched and held at 130 °C or 200 °C for 1 minutes in an oil bath. These samples were then reheated to 450 °C in a salt bath solution, and partitioned in thus solution for partitioning times varying from 1 minutes to 1 hour, followed by a water quench to RT, as shown in Figure 2.

These Q&P heat treatments were performed using Lenton UAF 14/27 and Carbolite HRF 7/22D furnaces with an estimated error on the temperature control of ± 5 °C. Thermocouples were used to maintain the oil bath temperature to ± 3 °C. Table II lists all the SS and DS Q&P heat treatment combinations tested and the nomenclature of each Q&P heat treatment to be used throughout the remainder of this paper. Only promising combinations were used for further study after this initial work.

C. Microstructural Analysis

X-ray diffraction (XRD) was used to determine which SS and DS Q&P heat treatments result in a detectable amount of RA for the purpose of TRIP to be achieved during deformation to delay necking and extend steel elongation. XRD was performed using a Bruker D8 Discover with a DaVinci Design diffractometer equipped with an Eiger2 R 500K laboratory area detector on cold-mounted cross sections of the steels identified in Table II. These mounts were ground using SiC papers from 400 to 2000 grit, and then polished with 3 and 1 μ m diamond suspensions in order to remove cutting damage and ensure enhanced detection of the RA prior to XRD scanning. A cobalt source in contrast to a copper source (λ_{avg} , Co = 1.79 Å versus λ_{avg} , Cu = 1.54 Å) was used to avoid Fe fluorescence in

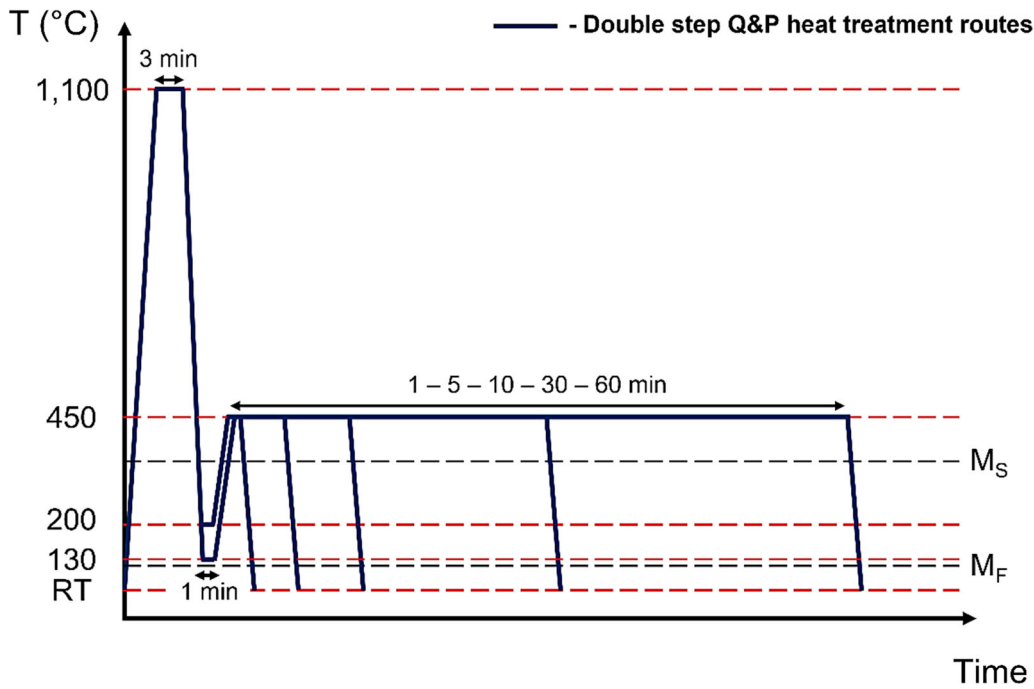


Fig. 2—Schematic representation of the experimental double-step (DS) Q&P heat treatments.

Table II. SS and DS Q&P Heat Treatments

Heat Treatment	Quench Temperature	Partitioning		Identification
		Temperature	Time	
DS Q&P	130 °C (oil)	450 °C (salt bath)	1 min	DS130-1
			5 min	DS130-5
			10 min	DS130-10
			30 min	DS130-30
			60 min	DS130-60
			60 min	DS130-60
DS Q&P	200 °C (oil)	450 °C (salt bath)	1 min	DS200-1
			5 min	DS200-5
			10 min	DS200-10
			30 min	DS200-30
			60 min	DS200-60
			60 min	DS200-60
SS Q&P	200 °C (oil)		1 min	SS-1
			5 min	SS-5
			10 min	SS-10
			30 min	SS-30
			60 min	SS-60
			8 h	SS-8h
			24 h	SS-24h
			48 h	SS-48h

this MSS. Triplicate measurements were made on separate areas per cold-mounted sample operating at 35 kV and 45 mA rotating between 40 and 120 deg (2θ) at a step size ($\Delta 2\theta$) of 0.01 deg and dwell time of 240 seconds per step. The collected 2D frames were then integrated with the aid of DIFFRAC.EVA software. The RA volume fraction was calculated with TOPAS software (Bruker AXS) using the (111), (200), and (220)

austenite peaks in accordance with the ASTM E975-13 standard.^[32]

For the transmission electron microscopy (TEM) examination, 2.0 mm diameter discs were punched and electropolished from steel sheets mechanically ground to a 100 to 120 μm thickness.^[33] A thermo-scientific Talos L120C TEM, equipped with a LaB6 filament operated at 120 kV, was used.

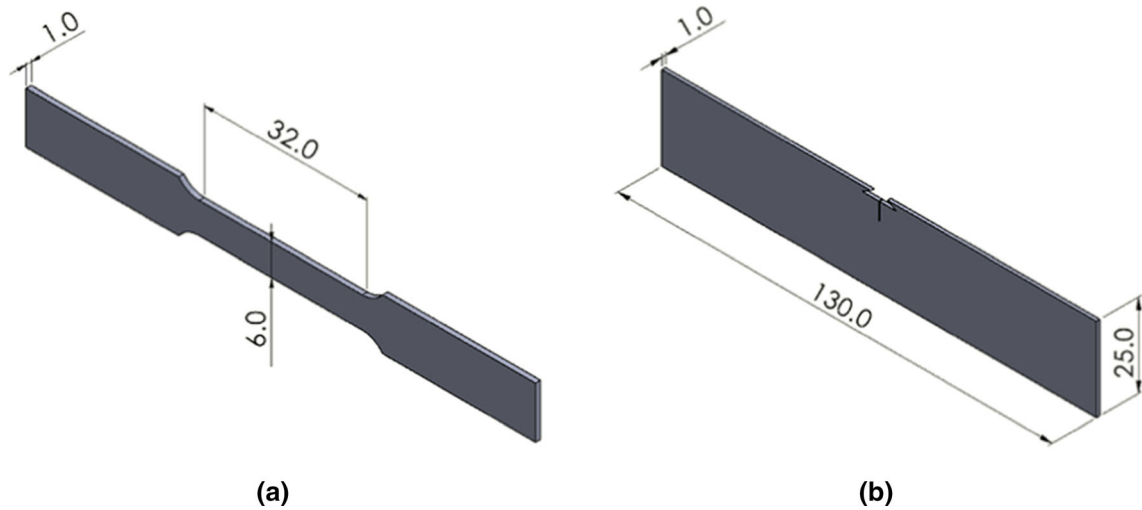


Fig. 3—(a) Standard sheet-type sample for tensile tests; and (b) clamped single-edge-notched-tensile (SENT) samples for fracture toughness tests. Nominal dimensions (in mm).

D. Mechanical Tests

Tensile testing was performed according to the ASTM E8/E8M 16-a standard^[34] in an MTS Alliance RT100 testing machine equipped with a tensile extensometer. The crosshead speed was 1.0 mm/min. Standard 1.0 mm thick, sheet samples with a width of 6 mm and a gauge length of 32 mm were used, as shown in Figure 3(a).

Current standards for fracture toughness tests recommend using samples with specific W/B ratios, allowing the use of any sample thickness if the requirements for testing are met, where W and B are the width and thickness of the specimen, respectively. In this context, fracture toughness tests were performed according to ASTM E1820-20b^[35] and BS 8571:2018^[36] standards using fatigue pre-cracked clamped SENT specimens, as shown in Figure 3(b). The tests were carried out on an MTS Landmark 370 servo-hydraulic testing machine equipped with a 25 kN load cell, hydraulic grips, and an MTS 632.02F-20 fracture extensometer. The samples were fatigue pre-cracked in air at RT with an applied frequency of 7 Hz and a load ratio of 0.1. The crack growth resistance curves in terms of the J -integral were determined using the unloading compliance technique.

The experimental results of the clamped SENT specimens were assessed in accordance with ASTM E1820-20b and BS 8571:2018a standards. The qualifying region for the J -crack extension (Δa) pairs of points was defined according to the BS 8571-18a standard, which recommends drawing an exclusion line parallel to the ordinate axis intersecting the abscissa at 0.2 mm and another one intersecting the abscissa at $0.2(W - a_0)$, where a_0 denotes the initial physical crack length. From the qualified data, a fitting procedure for the crack growth resistance curve determination, in terms of J -integral (J - R curve), was applied following the BS 8571-18a standard, and the initiation fracture toughness was determined at the intersection of the fitted J - R curve and the 0.2 mm crack extension auxiliary line ($J_{0.2}$). Checks for a possible qualification of $J_{0.2}$ as J_{Ic}

according to the ASTM 1820 standard were performed as follows:

$$B > 10 \frac{J_{0.2}}{\sigma_Y}, \quad [1]$$

where

$$\sigma_Y = \frac{(YS + UTS)}{2}. \quad [2]$$

The corresponding $K_{J0.2}$ values calculated from $J_{0.2}$ results as^[35]

$$K_{J0.2} = \sqrt{\frac{J_{0.2}E}{(1-\nu^2)}} \quad [3]$$

were also reported.

III. RESULTS AND DISCUSSION

A. Dilatometric Analysis of Q&P Heat Treatments

The martensite-to-austenite transformation during heating is accompanied by a volume contraction, which forms inflection points on dilatometric curves during heating.^[37] From the dilatometry results shown in Figure 4, the Ac_1 is 848 °C and the Ac_3 is 900 °C. When heating above the Ac_3 , the volume continues to increase, which also corresponds to the progressive dissolution of carbides in austenite as stated by Andrés *et al.*^[38] After carbide dissolution, it is necessary to hold the steel at the austenitization temperature to enable sufficient carbon diffusion and reduce the carbon concentration gradient across phase boundaries. This minimizes the possibility of carbide formation upon quenching and therefore reduces the deleterious effect that carbides situated on phase boundaries can have on the steel's mechanical properties. The austenitization temperature selected to encourage carbon diffusion and obtain a uniform distribution of

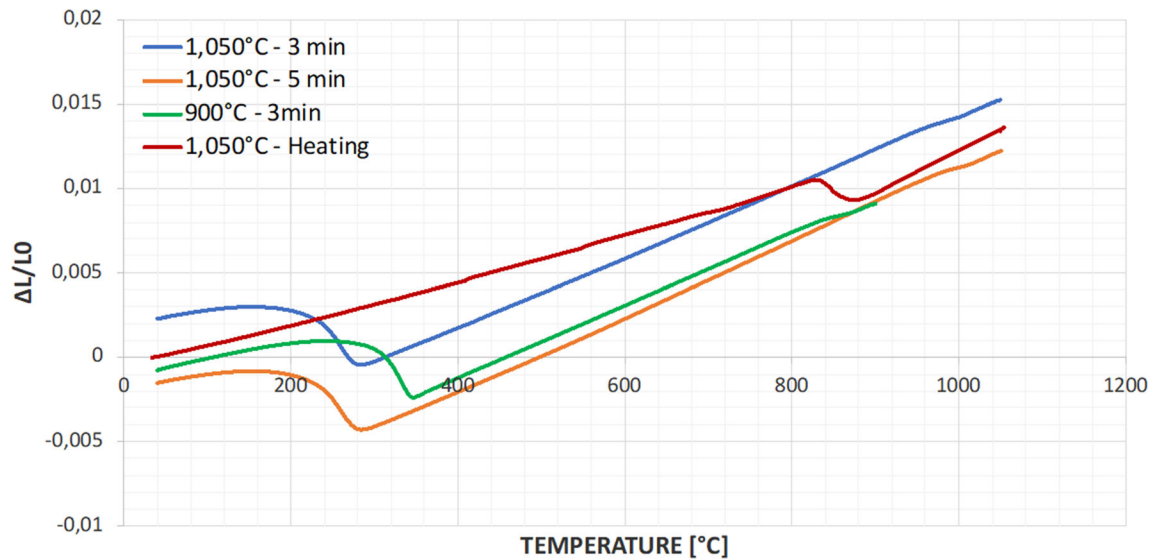


Fig. 4—Exemplificative curves: A_{c1} and A_{c3} temperatures found through heating ramps, M_s and M_f found through cooling ramps (dilatometry).

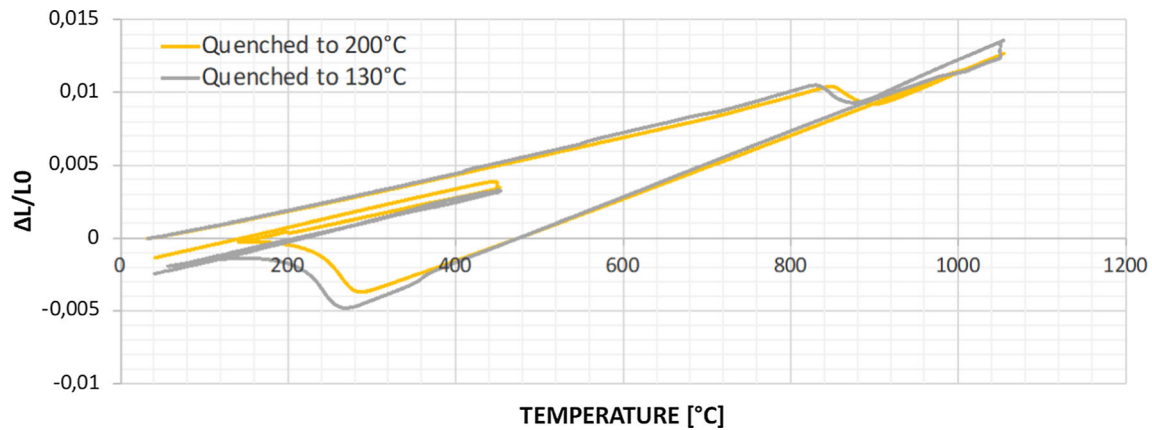


Fig. 5—Q&P dilatometry of samples quenched to 130 °C and 200 °C and then partitioned for 30 min (DS130-30 and DS200-30).

carbon in the microstructure was set to 1100 °C since higher temperatures could cause oxidation and degradation of the alloy.^[39,40]

Investigations carried out on various holding times at the selected austenitization temperature of 1100 °C showed that the holding time does not affect the M_s temperature,^[41,42] however 3 minutes was used to avoid excessive oxidation. Repeated heating and cooling cycles on select samples did not show changes to the A_{c1} , A_{c3} , M_s , and M fraction of this MSS. For the 1100 °C austenitization temperature, the M_s was found to be 270 °C and the M_f 130 °C.^[43]

For the AISI 420A low carbon MSS, holding at the chosen quench interruption temperatures of 130 °C and 200 °C did not cause changes to the expected linear thermal expansion graph as shown in Figure 5. This indicates that these temperatures are appropriate for partitioning as they do not cause undesired phase changes in the alloy.

Koistinen and Marburger defined a relationship, as stated in Eq. [3], to estimate the M fraction at a specified

quench temperature for a wide collection of steels with 0.3 to 1.1 wt pct C and RA of 0.6 to 18 vol pct. The fraction of M transformed is proportional to the degree of undercooling below M_s and is not dependent on time because the martensitic transformation is diffusionless.^[44]

$$f_m = 1 - e^{-\alpha_m(M_s - T_q)}, \quad [4]$$

where f_m is the austenite fraction that transforms to martensite upon quenching to a temperature T_q below the M_s temperature and α_m is the rate parameter (1.1×10^{-2}).^[3,42]

Using the Koistinen–Marburger relationship, less than 43 pct RA fraction was detected for each quenching interruption temperature, 200 °C and 130 °C, as shown in Table III. As a result, the M_s will be lower than RT and no fresh M is expected to form in accordance with Mola and De Cooman.^[45] For this reason, enough RA remains in the matrix after partitioning with the expectation that toughness can be enhanced.

B. Q&P Heat Treated Samples

1. XRD analysis

Using XRD, the highest RA levels were found in the DS130 and DS200 samples partitioned for 30 minutes at a partitioning temperature of 450 °C, as shown in Figure 6. RA is maximized at this intermediate DS Q&P heat treatment time because partitioning for less than 10 minutes does not permit sufficient carbon diffusion for RA stabilization, while partitioning for longer than 30 minutes allows carbide precipitation which reduces the C availability for RA stabilization.^[45] The overlap of error bars between the DS130 and DS200 samples in Figure 6 are shown at lower partitioning times (1 to 10 minutes), suggesting the effect of RA content with slight modifications in quench temperature at partitioning times, ≤ 10 minutes, is negligible. Ultimately, similar amounts of RA were detected at RT for both DS Q&P heat treatments at all partitioning times tested. As stated by Mola and De Cooman,^[45] the stabilization of the RA can also be assisted by local carbon enrichment, locking potential M nucleation sites at austenite/martensite (A/M) boundaries, and by austenite lattice defects formed as a result of the cooling rate.

As was expected, little to no RA in the SS Q&P heat treated samples partitioned for from 1 to 60 minutes was detected. This is because sufficient carbon enrichment and subsequent long-range diffusion in RA requires more time

at the lower SS partitioning temperature of 200 °C. The maximum amount of RA was found in the SS-8h sample, with lower RA values for longer partitioning times.

RA XRD peaks belonging to the (111) family of all SS and DS Q&P heat treatments with a considerable amount of RA are shown in Figure 7. RA XRD peaks belonging to the (200) and (211) families showed similar trends in peak behavior at different partitioning times. Table IV summarizes the total measured RA volume fraction in vol pct, the calculated RA lattice parameter, and the average carbon content in RA.

The RA lattice parameter and its respective carbon content were calculated using the combined equations of Ruhl and Cohen, and Dyson and Holmes.^[46] The RA carbon contents in the DS130-30 and DS200-30 samples (0.99 and 0.9 wt pct respectively) suggests that the chemical stability of RA is affected by quench temperature. In terms of partitioning time, the 30 minutes heat treatments allowed enough time for carbon to widely diffuse through the RA lattice, promoting chemical stability of RA, rather than forming carbides. However, this greater variation in (111) peak shifting illustrated in Figures 7(b) compared to (a), suggests that time has a greater impact on chemical stability of RA in the DS Q&P heat treated samples quenched at a higher temperature (200 °C) versus those quenched at slightly lower temperature (130 °C). Similarly, the SS Q&P heat treated samples also showed a wide variability in (111) peak shifting, as shown in Figure 7(c). The SS-8h sample, quenched and partitioned at 200 °C, revealed the highest carbon content of 1.54 wt pct out of all DS and SS Q&P heat treatments tested.

The Full Width at Half Maximum (FWHM) in Table IV of the (111) peak was determined using Origin 2020 software to assess peak broadening and to crudely calculate the average RA crystallite size resulting from these Q&P heat treatments using Scherrer's equation.^[47] Figure 7(c) as

Table III. Volume Fractions of RA (f_A) and Martensite (f_M) During Different Quench Interruption Temperatures

f_A	f_M	Temperature (°C)
1.00	0.00	284.9
0.39	0.61	199.7
0.18	0.82	129.2

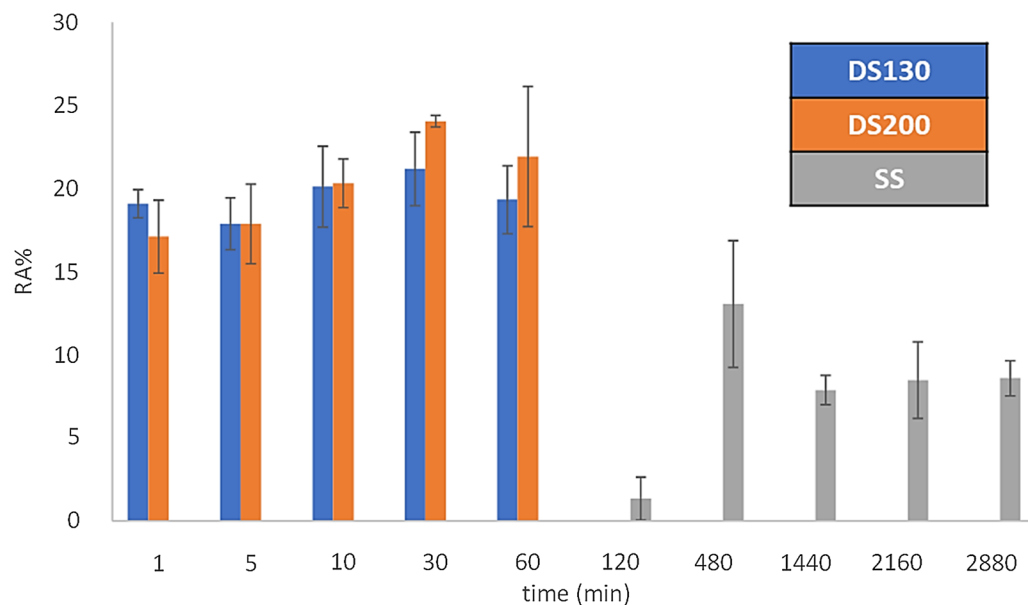


Fig. 6—Volume fraction of RA for all DS130, DS200 and SS Q&P heat treatments trialed. The error bars are plotted to a 90 pct Confidence Interval. The SS-2 h sample showed the least amount of RA (~ 1 pct) and therefore was eliminated from further analysis.

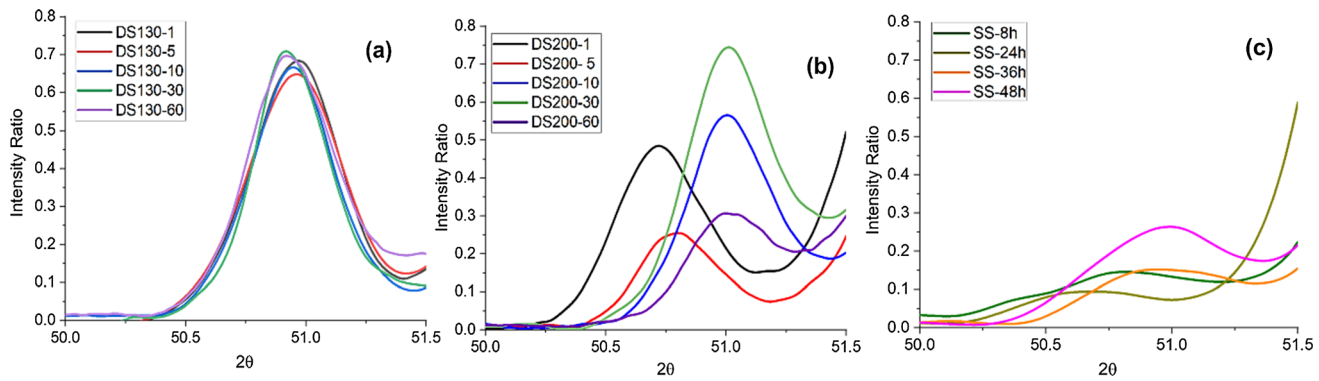


Fig. 7—RA XRD peaks belonging to the (111) family with a considerable amount of RA: (a) DS130; (b) DS200; (c) SS; Q&P heat treatments.

Table IV. Summary of RA Detected and Its Corresponding Calculated Crystal Parameters for DS130 and DS200 Samples Partitioned for 1 min to 1 h and for SS Samples Partitioned for 8 to 48 h

Time (min)	RA (Vol Pct)	RA Lattice Parameter (\AA)	C Content in RA (Wt Pct)	Peak Center (2θ)	FWHM	RA Crystallite Size (nm)
DS130						
1	19.09 \pm 0.84	3.61	1.03	50.97	0.46	23.34
5	17.89 \pm 1.55	3.60	0.96	50.96	0.48	22.05
10	20.12 \pm 2.44	3.61	1.05	50.95	0.41	26.04
30	21.19 \pm 2.21	3.60	0.99	50.92	0.38	27.82
60	19.39 \pm 2.05	3.61	1.05	50.92	0.45	23.89
DS200						
1	17.12 \pm 2.19	3.60	0.96	50.72	0.46	23.17
5	17.88 \pm 2.39	3.60	0.76	50.77	0.44	24.35
10	20.32 \pm 1.47	3.60	0.94	50.99	0.40	26.44
30	24.06 \pm 0.35	3.60	0.90	51.01	0.42	25.27
60	21.93 \pm 4.21	3.60	0.80	51.00	0.51	20.77
SS						
8 h	13.06 \pm 3.82	3.62	1.54	50.84	0.86	12.37
24 h	7.89 \pm 0.87	3.61	1.12	50.65	0.70	15.30
36 h	8.48 \pm 2.29	3.61	1.11	50.92	0.70	15.26
48 h	8.60 \pm 1.05	3.61	1.11	51.01	0.76	14.11

The full width at half maximum (FWHM) was calculated for the RA (111) peak. Similar trends in FWHM for the RA (200) and (211) peaks were observed.

well as Table IV shows that the SS Q&P heat treatments have the broadest peaks, and overall smaller RA crystallites ranging from 12.4 to 15.3 nm. By comparison, the DS Q&P heat treated samples had calculated RA crystallites ranging from 20.1 to 28.0 nm in size. This larger size is likely due to the higher partitioning temperature in the DS Q&P heat treatments (450 °C vs. 200 °C). Higher partitioning temperatures can enhance carbon diffusion, improving the RA's chemical stability but can also increase RA size thereby reducing its mechanical stability. In the SS Q&P heat treated samples, the quench and partitioning temperature is 200 °C. Carbon diffusion at this lower partitioning temperature is limited to nearby RA and therefore leads to a small fraction of stable RA in the microstructure.^[48,49] However, partitioning at the lower temperature of 200 °C, maintains the high mechanical stability with RA's small crystallite size in the SS Q&P heat treated samples.

2. TEM investigation

A comparative assessment of nanoscale microstructural features between the SS and DS Q&P heat treatments was performed on selected samples. The

chemical stability of RA is governed by the temperatures and times used in the SS and DS Q&P heat treatments while the mechanical stability of RA is governed by morphology. Figure 8 shows TEM images for the SS-24 h Q&P heat treated sample. As can be observed, the M laths are organized parallel to each other. Despite the known presence of RA at long partitioning times detected with XRD, RA thin-films are homogeneously distributed around M laths. The average film thickness is < 50 nm and length \leq 500 nm. At a 200 °C partitioning temperature, in which the SS Q&P heat treatment was carried out, carbon is supposed to partition in the RA or trapped at dislocations (Figure 8(e)) and grain boundaries act as a reservoir for carbon atoms. During partitioning, carbon diffuses from dislocations, causing a dislocation recovery process. It is also possible, apart from partitioning temperature, that the long partitioning times performed on the SS Q&P heat treated samples enabled an increase in the M lath volume fraction from the coarsening of these M laths and a homogeneous distribution of RA.^[21] Approximately 300 nm long, fine, and unevenly distributed carbides

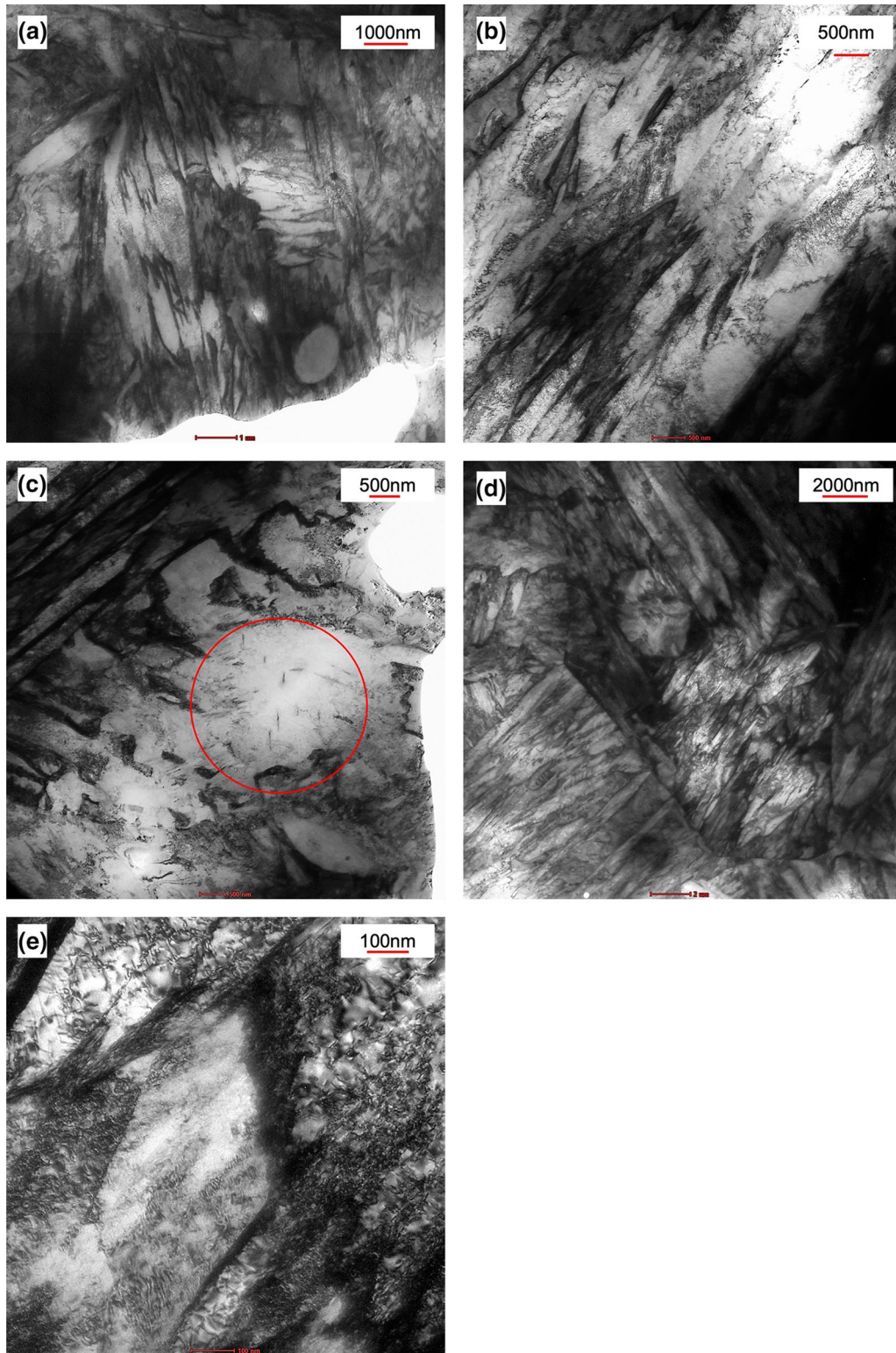


Fig. 8—TEM imaging of the SS Q&P heat treated sample (SS-24 h): (a) grain organization at a low magnification; (b) lath with same orientation, carbides precipitation, thin-film RA; (c) blocky austenite; (d) blocky RA at a low magnification; (e) Dislocations visible at a high magnification the SS Q&P sample, probable retained austenite (darker zone).

are visible further from M laths having two principal orientations. This is most likely because carbide formation is not favorable at this low partitioning

temperature. These nanoscale carbides observed could be advantageous in increasing the steel's yield strength.

The TEM analysis performed on the DS130-10 sample is shown in Figure 9. Figure 9(a) confirms that

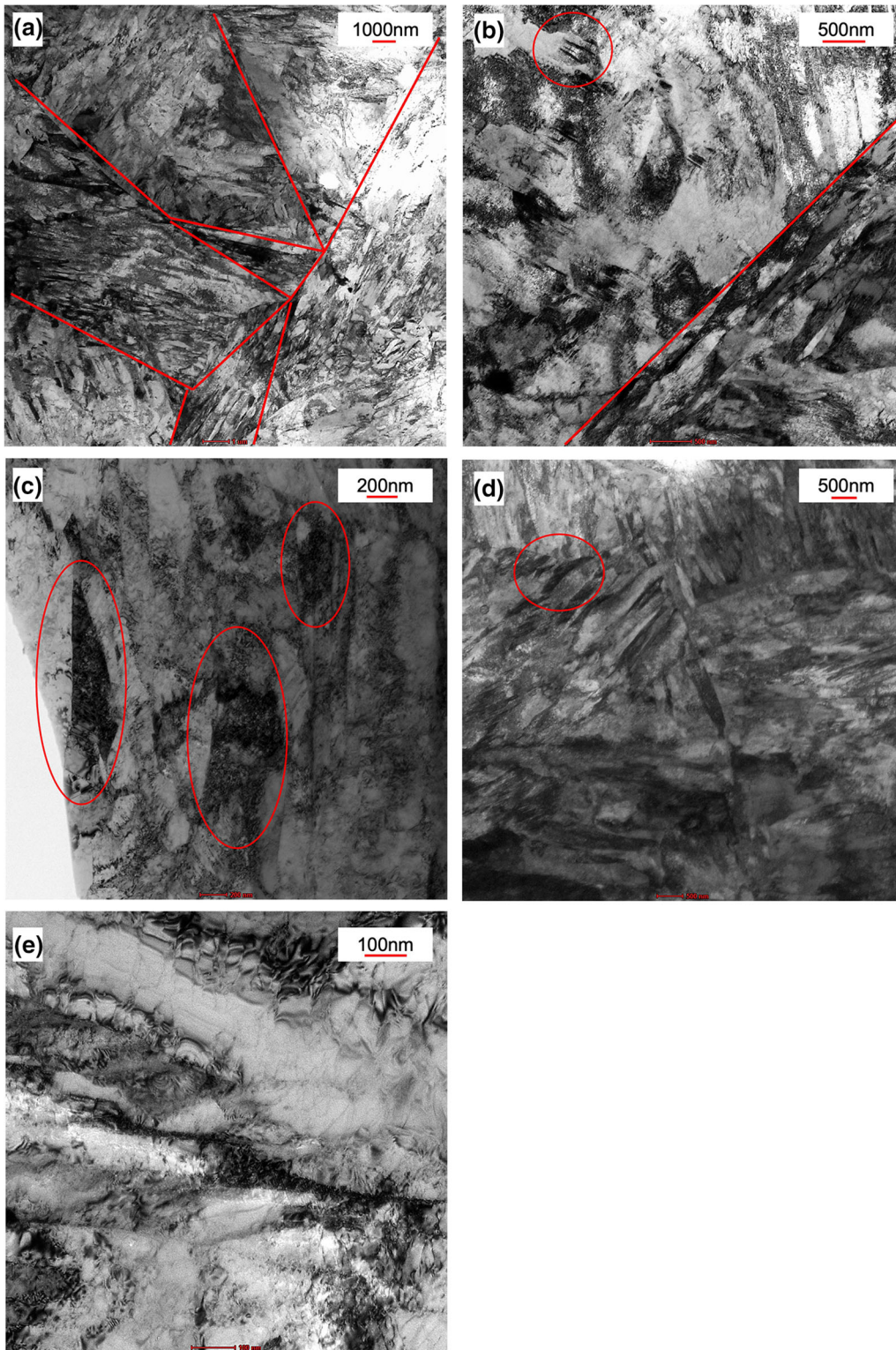


Fig. 9—TEM imaging of the DS Q&P heat treated sample (DS130-10): (a) grain organization at a low magnification; (b) lath with same orientation, carbides precipitation, RA thin-films; (c) blocky RA; (d) blocky RA at a low magnification; (e) Dislocations visible at a high magnification in the DS Q&P sample, probable retained austenite (darker zone).

M laths are arranged in randomly oriented packets in coarse grains, while unidirectional martensitic growth is observed in fine grains. Within a packet, groups of laths

with small misorientations (~ 10 deg) are collectively considered as blocks, whereas each group of laths is considered as sub-blocks.^[50,51] RA is mainly situated

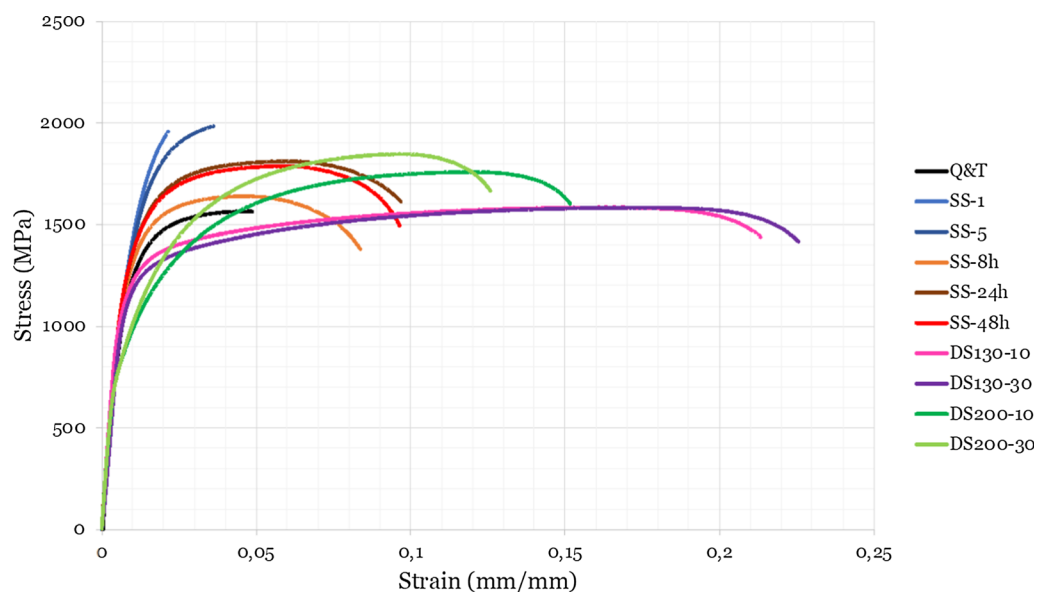


Fig. 10—Stress–strain curves for select DS and SS Q&P heat treated samples.

among sub-blocks with a thin-film morphology (Figures 9(a) and (b)). Apart from orientation, the growth direction of M lath is governed by the local stresses and the subsequent energy balance between the chemical gradient and strain energies. The M laths grow in directions that minimize those stresses, as stated by Yeddu.^[52,53]

The DS130-10 sample's microstructure shown in Figure 9 is mainly composed of M packets enclosed in prior austenite grains, as can be seen in Figure 9(a). Each grain presents a disorganized microstructure, while globally the DS130-10 sample has a multi-scaled composition. M packets contain blocks and sub-blocks, in which mostly plates with some laths are included. This is the result of the first part of the Q&P heat treatment from austenitization (1100 °C) to the chosen quench interruption temperature (130 °C). Parallel M laths of similar dimensions, as shown in Figures 9(a) and (d), indicates that the local stresses induced by the martensitic transformation were of the same magnitude and direction. In the bottom right corner of Figure 9(b), a non-uniform distribution of RA films surrounding an M lath were observed. The average thickness of these RA thin-films is < 50 nm and their length is approximately 500 nm. The block-type RA in Figure 9(c) measures 200 nm in width and 500 nm in length. RA is mostly situated on grain boundaries (Figure 9(a)) and dislocations (Figure 9(c)). Dislocations can form during the martensitic transformation upon quenching and its associated increase in volume generates dislocations in the neighboring austenite. The TEM analysis is consistent with Mola and De Cooman,^[45] who stated that stacking faults and dislocations are common observations in the RA of Q&P heat treated samples (Figure 9(e)).

The presence of carbides within the martensitic matrix is shown in the upper-left portion of Figure 9(b) which formed during partitioning. These carbides were measured to be approximately 300 nm in length, making it

submicron size advantageous in terms of increasing the steel's yield strength, as stated by Wendler *et al.*^[17]

The microstructure of the SS Q&P heat treated samples differs from the DS Q&P heat treated samples by the fact that M laths prevail and the whole structure is more homogenous. The SS Q&P heat treated microstructure presents a more homogeneous distribution of RA thin-films. The heterogeneity captured in the TEM examination of the DS Q&P heat treated sample, as shown Figure 9, is most likely a consequence of the lower quench interruption temperature (130 °C vs 200 °C) and shorter partitioning times tested. Moreover, in contrast to the SS Q&P heat treated samples, tempered M prevailed in the DS Q&P heat treated samples.

The carbon diffusion velocity in austenite is three orders of magnitude smaller than that in M.^[54] This means that carbon leaves the M phase rapidly and accumulates at the A/M boundary producing a segregation of carbon atoms. This implies, and has been experimentally shown previously with the use of in-situ tensile testing coupled with EBSD,^[55] that block-type RA blocks less stable than thin-film RA in a DS Q&P heat treatment. This explains the increased RA crystallite sizes determined in the XRD analysis of Table IV. In the SS Q&P heat treatment, RA remains along M laths. Even though carbon in austenite diffuses at a generally lower rate than in M, after 24 h of diffusion, thin-film RA are carbon-enriched. Thin-film RA situated at grain boundaries are at a particular advantage because carbon already accumulates naturally in this area therefore decreasing its length of diffusion in the RA. Carbides of the SS Q&P heat treated samples are thinner than those formed in the DS Q&P heat treated samples and are not surrounded by dislocations. The inter-carbide spacing was also measured to be shorter in the SS Q&P heat treated samples.

Table V. Average Mechanical Properties of the SS and DS Q&P Heat Treated Samples

Heat Treatment	YS (MPa)	UTS (MPa)	<i>E</i> Pct	UTS (MPa) × <i>E</i> Pct
DS130-10	1082	1585	21.2	33,602
DS130-30	1093	1584	22.4	35,482
DS200-10	796	1759	15.0	26,385
DS200-30	792	1847	12.6	23,272
SS-1	1256	1963	2.6	5104
SS-5	1218	1984	3.6	7142
SS-8 h	1126	1641	8.4	13,784
SS-24 h	1188	1812	9.7	17,576
SS-48 h	1195	1790	9.7	17,363
Q&T (400 °C*)	1303	1565	4.5	7042

*Tempering temperature

Table VI. Experimental Fracture Toughness Values of Q&P and Q&T Samples

Heat Treatment	SS-24 h		DS130-10		DS130-30		DS200-10		Q&T (400°C)
Sample No.	I	II	I	II	I	II	I	II	I
$J_{0.2}$ (kJ/m ²)	16.6	22.0	56.7	56.8	77.0	61.0	19.8	24.3	19.5
$K_{J0.2}$ (MPa m ^{1/2})	61.9	71.3	114.4	114.5	133.3	118.6	67.6	74.9	67.1

3. Tensile properties

Select engineering stress-strain curves of SS and DS Q&P heat treatments as well as a conventional Q&T heat treatment (at 400 °C for 15 minutes) of the AISI 420A low carbon MSS, for comparison, are reported in Figure 10. The average values of yield strength (YS), UTS and *E* pct, obtained from three samples for each condition are listed in Table V. The strength-ductility balance of each SS and DS Q&P heat treatment was evaluated by the product of the UTS and *E* pct (UTS × *E* pct) also shown in Table V. All stress-strain curves in Figure 10 show continuous work hardening from the YS up to the UTS, as observed typical in high-strength Q&P steels.^[23,56,57] Rather this continuous work hardening behavior could be indicative of the simultaneous activation of dislocation motion and TRIP promoting improved ductility.^[58]

The DS130-10 and DS130-30 samples showed similar tensile mechanical properties. This is an expected result from the similar RA volume fractions detected in the XRD analysis, with the DS130-30 sample showing a marginal improvement in *E* pct. These samples showed the highest *E* pct from 21.2 to 22.4 pct out of all Q&P heat treatments tested. This indicates that the RA microstructural heterogeneity found through the TEM analysis did not play a detrimental role in limiting the steel's *E* pct. On the contrary, the tempered M and the possibility of gradual TRIP exhaustion of block-type RA^[55] within the DS130 Q&P microstructure improved the steel's *E* pct. In comparison, the DS200 Q&P heat treated samples exhibited lower *E* pct compared DS130 Q&P heat treated samples (15.0/12.6 pct vs. 21.2/22.4 pct). However, this reduction in *E* pct is compensated by

a slight increase in UTS (1759/1847 MPa vs. 1585/1584 MPa) maintaining a high strength-ductility balance of the steel.

The DS200-10 samples showed an *E* pct approaching 15.0 pct, while the DS200-30 samples showed an *E* pct of 12.6 pct, even though the DS200-30 samples showed a slightly greater amount of RA in comparison with the DS200-10 sample. The YS attained was approximately 800 MPa for both DS200 partitioning times tested.

Shorter partitioning times of the SS-1 and SS-5 samples exhibited the highest strengths, 1812 MPa and 1,790 MPa and lowest *E* pct, 2.6 and 3.6 pct, respectively out of all SS and DS Q&P heat treatments tested. Nevertheless, SS Q&P heat treatments were able to achieve an *E* pct of 9.7 pct at long partitioning times (24 and 48 hours) with similar values of YS and UTS. It is interesting to note that the SS-8 h samples resulted in lower UTS and *E* pct values in comparison to the SS-24h and SS-48h samples despite achieving the highest RA volume fraction from the XRD analysis in Table IV. It can be explained due to the higher carbon enrichment of RA in this condition. However, it is most reasonable to consider the sample partitioned for lesser time, 24 hours, as the more efficient Q&P heat treatment for industrial practices among the SS Q&P heat treatments.

All DS Q&P heat treatments tested, showed a significant improvement in *E* pct with a quite similar UTS compared to the Q&T heat treated samples. Compared to the 4.5 pct *E* pct exhibited by the Q&T samples, the SS Q&P samples showed an *E* pct varying from 2.6 to 9.7 pct while the DS Q&P samples showed higher *E* pct values, varying from 12.6 to 22.4 pct.

4. Fracture toughness

The experimental fracture toughness of $J_{0.2}$ and $K_{J0.2}$ resulting from the different SS and DS Q&P heat treatments, are listed in Table VI. The results from one Q&T sample were also included as a reference. Checks for the possible qualification of $J_{0.2}$ as J_{Ic} according to the ASTM 1820 standard were performed, and the requirements related to the specimen thickness for considering $J_{0.2}$ as J_{Ic} were met. As a result, the reported $J_{0.2}$ values as defined by the BS 8571 standard were considered to be the fracture toughness of the material, which is a size-independent mechanical property. As can be seen, the highest fracture toughness was attained by the DS130 Q&P heat treated samples. The DS130-30 samples showed slightly higher $J_{0.2}$ values in comparison to the DS130-10 samples. The DS200-10 samples did not exhibit high fracture toughness when compared with the SS-24h samples, despite having a higher volume fraction of RA, as shown in Table IV.

According to Tables IV and VI, the Q&P heat treatments with the highest fracture toughness were those with higher contents of RA (DS130-30 with 20 vol pct of RA). Even though similar volume fractions of RA were detected in the DS130-10 and DS200-10 samples, the fracture toughness of the DS200-10 samples was approximately half of that of the DS130-10 samples. The DS200 Q&P heat treated samples presented higher volume fractions of RA with respect to the SS Q&P heat treated samples; however, interestingly, their fracture toughness is comparable.

C. Discussion Summary

The microstructural and mechanical effects of SS and DS Q&P heat treatments on an AISI 420A low carbon MSS has been studied. Quench interruption temperatures (130 °C and 200 °C) and holding times were obtained by ThermoCalc simulations and dilatometry. The final microstructure is composite-like comprised of M laths, M plates, RA thin-films, as well as nanoscale carbides. The amount of RA obtained experimentally is lower than that predicted by the Koistinen–Marburger relationship: the high Cr-level in this alloy may have hindered carbon from diffusing to chemically stabilizing RA, thus forming carbides and decreasing the thermodynamic activity of carbon as estimated by Tsuchiyama *et al.*^[10] These carbides, as illustrated in Figures 8 and 9, are 300 nm in length for both the SS and DS Q&P heat treatments but in the former case their formation was most likely hindered by the low partitioning temperature of 200 °C. The formed carbides are predominantly nanosized and, therefore, strengthen the alloy, as reported by Tariq and Baloch.^[8] Another factor that can reduce the final RA volume fraction is the possibility of fresh M formation after partitioning. The enrichment of carbon in RA could have been impeded both by the carbide formation and the low carbon diffusion velocity in RA as stated in the TEM analysis.

From the DS130 and DS200 samples tested, it is clear that a quench interruption temperature of 200 °C is too high for an effective DS Q&P heat treatment as it reduces the steel's E pct and fracture toughness, as

shown in Tables V and VI, respectively. The volume fraction of RA detected was similar for both quench interruption temperatures (130 °C and 200 °C) of the DS Q&P heat treatment, but the stability of RA is evidently different. The higher quench temperature forms an insufficiently widespread martensitic matrix in the microstructure, which decreases the amount of carbon available for partitioning into RA and increases its size. The DS200 samples exhibited the lowest average carbon content in RA and largest RA crystallite size as shown in Table IV. This prevents the RA in the DS200 samples from being an effective toughening phase and therefore activates TRIP rapidly upon straining. Austenite stabilization is not only governed by its *uniform* carbon enrichment, but also by *local* carbon enrichment blocking potential M nucleation sites in the bulk austenite and at A/M phase boundaries. This mechanism is more common at low quench temperatures, because of higher primary M fractions that strengthen more RA.^[45]

It is evident that even a small amount of RA, introduced at short partitioning times is enough to increase the strength-ductility balance of this steel. With the DS Q&P heat treated samples, partitioning from 10 and 30 minutes at 450 °C, as shown in Table V, very easily increased the strength-ductility balance by approximately 3 times with 20 to 24 vol pct of RA introduced in the microstructure, as noted in Table IV, in comparison to the Q&T heat treated samples. For example, the DS200-10 heat treatment exhibited a strength-ductility balance of 26,385 MPa pct which is 4 times more than the Q&T heat treatment with a strength-ductility balance of 7042 MPa pct. More importantly, DS Q&P heat treating of this 1 mm thick, sheet of MSS meets the general strength-ductility balances ($24,000 \text{ MPa pct} \leq \text{UTS} \times \text{TE} \leq 40,000 \text{ MPa pct}$)^[59] required by the US DoE for 3rd generation Advanced High Strength Steels to be incorporated in future vehicles. From Table V, and comparing the SS samples partitioned for a short amount of time (SS-1 and SS-5, respectively) to the Q&T sample, the strength-ductility balance is increased by approximately the same.

A promising SS Q&P heat treatment for industrial practice is the SS-24h treatment, which shows a high strength-ductility balance of UTS, E pct, and $\text{UTS} \times E$ pct of 1,812 MPa, 9.7, and 17,578 MPa pct, respectively, as shown in Table V. The high UTS value is probably related to the combination of a high quench and low partitioning temperature, whereas the improved E pct is due to the introduction of RA into the microstructure of the steel. Ultimately, the SS Q&P heat treatments performed on this MSS shows the potential to achieve an E pct of 12 pct and strength-ductility balance ranging from 14,000 to 17,000 MPa pct.

As stated previously, a high quench temperature leads to form a greater amount of RA but, in this case, the partitioning temperature in the SS samples is too low to enhance the diffusion of carbon into RA, even with a long partitioning time. This leads to reduced carbon mobility in which only RA thin-films, as shown in Figure 8, near M laths are chemically stabilized. The

mechanical stability, on the other hand, of the RA is maintained as a result of its small size, as crudely assessed in Table IV and shown in Figure 8, after carbon enrichment. The unstable RA not in the vicinity of M laths in these SS Q&P heat treated samples becomes fresh M after the final quench. As stated in Reference 60, this kind of M reduces the steel's ductility.

The volume fraction of RA does not seem to play a critical role in the fracture toughness. The reported fracture toughness values may be influenced by the distribution of RA in the microstructure, nanoscale transitional carbides, and the fraction of fresh and tempered M. The fracture behavior of both the SS and DS200 samples was associated with the fresh M, which did not have time to temper and was maintained as a brittle phase. The fracture toughness values of the SS and DS Q&P heat treated samples were comparable to those of the Q&T samples tempered at 400 °C, 67 MPa m^{1/2}, and to those of Q&T AISI 420 steel found in the literature (49 MPa m^{1/2}).^[61] In this case, RA balances the effect of untempered M on the test results. In contrast, the DS130 samples featured the highest fracture toughness values, and the $J_{0.2}$ and $K_{J0.2}$ of these samples were almost double of the SS samples. The DS130 samples showed similar RA volume fractions to the DS200 samples, but the fraction of M formed during quenching was higher in the former case. This allowed the DS130 samples to present more carbon available for RA chemical stabilization during partitioning. Indeed, the carbon content in RA was slightly higher in this case (Table IV). For these reasons, RA is more stable, and the TRIP effect is delayed, thereby reducing the possibility of crack tip embrittlement and low fracture toughness.^[52] Nonetheless, the most industrially relevant partitioning times studied were between 10 and 30 min for the DS Q&P heat treated samples, as shown in Figure 11. DS130 samples exhibited the highest values in terms of the resulting E pct (22 pct), UTS (1,585 MPa), and fracture toughness ($J_{0.2} = 77$ kJ/m² and $K_{J0.2} = 133$ MPa m^{1/2}). Moreover, the current limitations of the novel SS Q&P heat treatments presented in this paper are related to the long partitioning time and low fracture toughness ($J_{0.2} = 22$ kJ/m² and $K_{J0.2} = 71$ MPa m^{1/2}); however, the advantages are linked to the low temperature and reduced number of heating/transfer cycles.

IV. CONCLUDING REMARKS

In this study, several unique SS and DS Q&P heat treatments were performed on a commercial AISI 420A low carbon MSS to optimize its mechanical properties. Based on the experimental results, the following conclusions can be drawn:

- The performed Q&P heat treatments proved to be effective in retaining a significant volume fraction of RA in MSSs. The DS Q&P heat treatments achieved higher volume fractions of RA ranging from 17 to 24 vol pct, while the SS Q&P heat treatments achieved volume fractions ranging from 13 to 8 vol pct. The

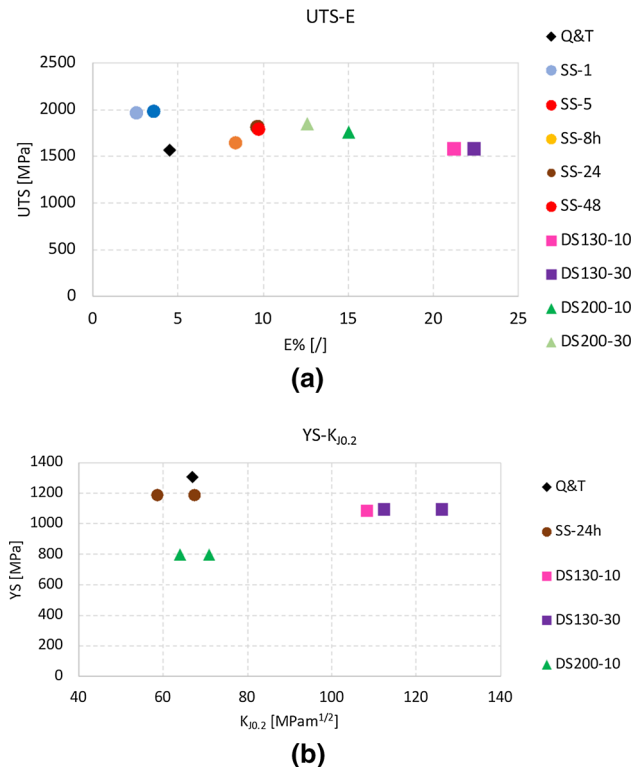


Fig. 11—UTS vs. E pct (a) and YS vs. $K_{J0.2}$ (b) chart for the different heat treatment.

greatest chemical stability and smallest crystallite sizes of RA, 1.54 wt pct C and 12 to 15 nm, was attained with a SS Q&P heat treatment.

- Competitive mechanisms (*i.e.* carbide formation) enhance the mechanical properties increasing the strength for a precipitation mechanism phenomena.
- The RA within the martensite matrix was considered the main cause of fracture toughness improvement of this MSS subjected to Q&P heat treatments.
- The AISI 420A MSS subjected to all SS and DS Q&P heat treatments maintain or improve the UTS in comparison to its traditional Q&T heat treatment, whilst improving its E pct.
- The DS130 Q&P heat treated samples partitioned for industrially relevant times ensured the most reliable MSS performance tested. These samples achieved an E pct of 22 pct, UTS of 1585 MPa, $J_{0.2} = 77$ kJ/m² and $K_{J0.2} = 133$ MPa m^{1/2}, suggesting that this treatment is promising for automotive applications.
- The best conditions achieved of this novel SS Q&P heat treatment resulted in an E pct of 8 to 10 pct, UTS of ~ 1650 to 1800 MPa, $J_{0.2} = 22$ kJ/m² and $K_{J0.2} = 71$ MPa m^{1/2}. A low fracture toughness was obtained at the cost of long partitioning time (24 hours), yet a significant improvement in UTS* E pct in comparison its traditional Q&T heat treatment was attained (17,576 MPa pct vs. 7,042 MPa pct). Ultimately, this work opens the possibility for MSSs to reach an E pct of 12 pct and strength-ductility balance ranging from 14,000 to 17,000 MPa pct

with the advantage of a reduced number of heating/transfer cycles.

FUNDING

Open access funding provided by Politecnico di Milano within the CRUI-CARE Agreement.

CONFLICT OF INTEREST

On behalf of all authors, the corresponding author states that there is no conflict of interest.

OPEN ACCESS

This article is licensed under a Creative Commons Attribution 4.0 International License, which permits use, sharing, adaptation, distribution and reproduction in any medium or format, as long as you give appropriate credit to the original author(s) and the source, provide a link to the Creative Commons licence, and indicate if changes were made. The images or other third party material in this article are included in the article's Creative Commons licence, unless indicated otherwise in a credit line to the material. If material is not included in the article's Creative Commons licence and your intended use is not permitted by statutory regulation or exceeds the permitted use, you will need to obtain permission directly from the copyright holder. To view a copy of this licence, visit <http://creativecommons.org/licenses/by/4.0/>.

REFERENCES

1. J.G. Speer, E. de Moor, and A.J. Clarke: *Mater. Sci. Technol. (United Kingdom)*, 2015, vol. 31, pp. 3–9.
2. T. Wu, R. Wu, B. Liu, W. Liang, and D. Ke: *Metals (Basel)*, 2019, <https://doi.org/10.3390/met9090958>.
3. J.G. Speer, E. De Moor, K.O. Findley, D.K. Matlock, B.C. De Cooman, and D.V. Edmonds: *Metall. Mater. Trans. A*, 2011, vol. 42A, pp. 3591–3601.
4. M. Frigo and S. Lindner: in *Proceeding of Me-Mo, Metals for raod mobility*, vol. 46, AIM, Bergamo, 2020, pp. 52–59.
5. H. Qu, G.M. Michal, and A.H. Heuer: *Metall. Mater. Trans. A*, 2014, vol. 45A, pp. 2741–49.
6. X.D. Wang, Z.H. Guo, and Y.H. Rong: *Mater. Sci. Eng. A*, 2011, vol. 529, pp. 35–40.
7. R. Venturini, A. Bianchi, M. Andraghetti, C. Guarnaschelli, M.C. Cesile, and P.E. di Nunzio: *La Metallurgia Italiana*, 2020, vol. 46, pp. 43–51.
8. F. Tariq and R.A. Baloch: *J. Mater. Eng. Perform.*, 2014, vol. 23, pp. 1726–39.
9. G.E. Totten: *Steel Heat Treatment: Metallurgy and Technologies*, CRC Press, Boca Raton, 2006.
10. T. Tsuchiyama, J. Tobata, T. Tao, N. Nakada, and S. Takaki: *Mater. Sci. Eng. A*, 2012, vol. 532, pp. 585–92.
11. H. Kong, Q. Chao, B. Rolfe, and H. Beladi: *Mater. Des.*, 2019, vol. 174, pp. 1–10.
12. J. Tobata, K.L. Ngo-Huynh, N. Nakada, T. Tsuchiyama, and S. Takaki: *ISIJ Int.*, 2012, vol. 52, pp. 1377–82.
13. J.G. Speer, F.C. Rizzo Assunção, D.K. Matlock, and Dv. Edmonds: *Mater. Res.*, 2005, vol. 8, pp. 417–23.
14. E.J. Seo, L. Cho, and B.C. de Cooman: *Metall. Mater. Trans. A*, 2016, vol. 47A, pp. 3797–3802.
15. Y. Hui Guo, Z. Yong Fang, Z. Min Wang, B. Fu, and X. Tao Deng: *J. Mater. Eng. Perform.*, 2019, vol. 28, pp. 3630–37.
16. Y.F. Shen, X.X. Dong, X.T. Song, and N. Jia: *Sci. Rep.*, 2019, vol. 9, pp. 1–9.
17. M. Wendler, C. Ullrich, M. Hauser, L. Krüger, O. Volkova, A. Weiß, and J. Mola: *Acta Mater.*, 2017, vol. 133, pp. 346–55.
18. Q. Huang, C. Schröder, H. Biermann, O. Volkova, and J. Mola: *Steel Res. Int.*, 2016, vol. 87, pp. 1082–94.
19. A.R. Entwisle: *Metall. Trans.*, 1971, vol. 2, pp. 2395–2407.
20. W. Steven: *J. Iron Steel Inst.*, 1956, vol. 183, pp. 349–59.
21. K.W. Andrews: *J. Iron Steel Inst.*, 1965, vol. 203, pp. 721–27.
22. M.J. Santofimia, L. Zhao, and J. Sietsma: *Metall. Mater. Trans. A*, 2011, vol. 42A, pp. 3620–26.
23. A. Sierra-Soraluce, G. Li, M.J. Santofimia, J.M. Molina-Aldarreguia, A. Smith, M. Muratori, and I. Sabirov: *Mater. Sci. Eng. A*, 2023, vol. 864, pp. 1–14.
24. S.J. Lee, D.K. Matlock, and C.J. Van Tyne: *Scr. Mater.*, 2011, vol. 64, pp. 805–08.
25. T. Suzuki, Y. Ono, G. Miyamoto, and T. Furuhashi: *ISIJ J.*, 2010, vol. 50, pp. 1476–82.
26. D.S. Codd: in *SAE 2011 World Congress and Exhibition*, 2011.
27. H. Chen, L. Zhao, S. Lu, Z. Lin, T. Wen, and Z. Chen: *Metals (Basel)*, 2022, vol. 12, p. 12.
28. S. Kang, K. Kim, Y. Il Son, and S.J. Lee: *ISIJ Int.*, 2016, vol. 56, pp. 2057–61.
29. A.A. Gorni: *Steel Forming and Heat Treating Handbook*, www.gorni.eng.br/e/Gorni_SFHTHandbook, 2019.
30. K. Harsha Vardhan, V. Shubhanyu, R. Kumar, and S. Abhishek: *Int. J. Current Eng. Technol.*, 2017, vol. 7, pp. 1–4.
31. A. Hanumantharaju: KTH, 2017.
32. ASTM International: *ASTM E975-13 Standard Practice for X-Ray Determination of Retained Austenite in Steel with Near Random Crystallographic Orientation*.
33. D.V.S. Rao, K. Muraleedharan, and C.J. Humphreys: *Microscopy*, 2010, vol. 2, p. 1232.
34. *ASTM E8M-Standard Test Methods for Tension Testing of Metallic Materials*, ASM International, 2021.
35. *ASTM E1820: Standard Test Method for Measurement of Fracture Toughness*, ASTM international, 2020.
36. *BS 8571:2018: Method of Test for Determination of Fracture Toughness in Metallic Materials Using Single Edge Notched Tension (SENT) Specimens*, British Standards Institute, 2018.
37. S.J. Lee and K.S. Park: *Metall. Mater. Trans. A*, 2013, vol. 44, pp. 3423–27.
38. C. García De Andrés, F.G. Caballero, C. Capdevila, and L.F. Álvarez: *Mater. Charact.*, 2002, vol. 48, pp. 101–11.
39. A.N. Isfahany, H. Saghafian, and G. Borhani: *J. Alloys Compd.*, 2011, vol. 509, pp. 3931–36.
40. Y.S. Choi, J.G. Kim, Y.S. Park, and J.Y. Park: *Mater. Lett.*, 2007, vol. 61, pp. 244–47.
41. Q. Huang, B.C. de Cooman, H. Biermann, and J. Mola: *Metall. Mater. Trans. A*, 2016, vol. 47A, pp. 1947–59.
42. S. Dieck, P. Rosemann, A. Kromm, and T. Halle: *IOP Conf. Ser.*, 2017, vol. 181, p. 12034.
43. R.A. Stewart, J.G. Speer, B.G. Thomas, E. de Moor, and A.J. Clarke: *Metall. Mater. Trans. A*, 2019, vol. 50, pp. 4701–13.
44. D.P. Koistinen and R.E. Marburger: *Acta Metall.*, 1959, vol. 7, pp. 59–60.
45. J. Mola and B.C. De Cooman: *Metall. Mater. Trans. A*, 2013, vol. 44A, pp. 946–67.
46. D.J. Dyson and B. Holmes: *J. Iron Steel Inst.*, 1970, vol. 208, pp. 469–74.
47. P. Scherrer: *Nachrichten von Der Gesellschaft Der Wissenschaften Zu Göttingen, Mathematisch-Physikalische Klasse*, vol. 2, 1918.
48. S. Ebner, R. Schnitzer, E. Maawad, C. Suppan, and C. Hofer: *Materialia (Oxf)*, 2021, vol. 15, pp. 1–10.
49. F.M. CastroCerdeira, E.I. Hernández, T. Ros-Yanez, and R.H. Petrov: *Metall. Mater. Trans. A*, 2020, vol. 51A, pp. 1506–18.
50. S. Morito, Y. Adachi, and T. Ohba: *Mater. Trans.*, 2009, vol. 50, pp. 1919–23.
51. S. Morito, H. Tanaka, R. Konishi, T. Furuhashi, and T. Maki: *Acta Mater.*, 2003, vol. 51, pp. 1789–99.
52. H.K. Yeddu: *Comput. Mater. Sci.*, 2018, vol. 154, pp. 75–83.
53. E.A. Ariza, J. Poplawsky, W. Guo, K. Unocic, A.J. Ramirez, A.P. Tschiptschin, and S.S. Babu: *Metall. Mater. Trans. A*, 2018, vol. 49A, pp. 4809–23.

54. L. Yuan: Rheinisch-Westfälischen Technischen Hochschule Aachen, 2012.
55. D. Salehiyan, J. Samei, B.S. Amirkhiz, L.G. Hector, and D.S. Wilkinson: *Metall. Mater. Trans. A*, 2020, vol. 51A, pp. 4524–39.
56. R. Eckner, L. Krüger, C. Ullrich, M. Wendler, and O. Volkova: *Int. J. Fract.*, 2019, vol. 215, pp. 139–51.
57. E. de Moor, S. Lacroix, A.J. Clarke, J. Penning, and J.G. Speer: *Metall. Mater. Trans. A*, 2008, vol. 39A, pp. 2586–95.
58. K.M.H. Bhadhon, J.R. Mcdermid, X. Wang, E.A. McNally, and F.E. Goodwin: in *Proceeding of the 11th International Conference on Zinc and Zinc Alloy Coated Steel Sheet GALVATECH*, Tokyo, 2017, pp. 1–8.
59. M. Takahashi: *ISIJ Int.*, 2015, vol. 55, p. 55.
60. E.I. Hernandez-Duran, T. Ros-Yanez, F.M. Castro-Cerda, and R.H. Petrov: *Mater. Sci. Eng. A*, 2020, vol. 797, pp. 1–2.
61. G. Prieto, W.R. Tuckart, and J.E.P. Ipiña: *Materiali in Tehnologije*, 2017, vol. 51, pp. 591–96.

Publisher's Note Springer Nature remains neutral with regard to jurisdictional claims in published maps and institutional affiliations.